DESIGN OF A QUASI-STEADY POWDER-BURNER TEST BENCH

A THESIS

Presented to the University Honors Program

California State University, Long Beach

In Partial Fulfillment

Of the Requirements for the

University Honors Program Certificated

Dararath Run

Fall 2025

I, THE UNDERSIGNED MEMBER OF THE COMMITTEE, HAVE

APPROVED THIS THESIS

DESIGN OF A QUASI-STEADY POWDER-BURNER TEST BENCH

By

Dararath Run

Joseph Kalman, Ph.D. (Thesis Advisor) **MAE Department**

California State University, Long Beach

Fall 2025

ABSTRACT

DESIGN OF A QUASI-STEADY POWERDER BURNER TEST BENCH

By

Dararath Run

December 2025

Hybrid gas-particle combustion is central to metallized propulsion concepts and to dust-explosion safety, yet there is a lack of small-scale burners that can generate well-characterized, quasi-steady dust clouds for detailed study. This work presents the design of a quasi-steady powder-burner test bench that injects controlled quantities of solid particles into a premixed methane-air stream while preserving optical access at the nozzle for flame imaging and diagnostics. The design process proceeded through four iterations focused on leakage control, manufacturability, sample-loading clearance, and reliable actuation. The final configuration uses a rigid three-post aluminum frame welded to a stainless-steel flow body, a flanged inlet for leak-tight connection to the gas supply, and a converging-diverging Venturi nozzle with a commercial micro-orifice that functions as an ejector-style mixer. Samples are introduced from below using a sealed container and piston driven by a variable-speed linear actuator mounted on a vertically sliding platform, which provides both precise control of the powder feed rate and sufficient clearance for safe sample loading. Torque requirements for the actuator were sized using O-ring contact and friction estimates to ensure motion under worst-case sealing loads. The resulting system delivers a complete, manufacturable design for the lower section of the test bench and defines mechanical and flow interfaces for future development of the upper flow-control and burner modules.

Table of Content

Chapter 1: Introduction and Theory

1.1 Background Theory

Combustion is the rapid, exothermic oxidation of a fuel, sustained by feedback of heat and active radicals to the unreacted mixture. Most engineering flames are deflagrations subsonic reaction waves whose propagation speed relative to the unburned mixture is the laminar burning velocity S_L. From stoichiometric methane-air at ambient conditions, Has a flame speed on the order of ~1 ft/s [10]. In hybrid gas-particle systems such as methane seeded with micron-scale aluminum, the premixed methane-air flame preheats and oxidizes the particles. At low metal loadings, the particles primarily act as a heat sink, thickening the flame and reducing the burning velocity. Beyond a critical aluminum concentration, however, the particle oxidation adds significant heat release so that the gas and dust phases couple and propagate as a single flame front [8]. This combustion regime is relevant to metallized solid propellants, metal-fueled power and heat-storage systems, reactive spray processing, and the assessment of gas-dust explosion hazards in industry.

Two canonical flame archetypes are premixed flames and non-premixed (diffusion) flames. In premixed flames, fuel and oxidizer are mixed prior to ignition, and the local equivalence ratio determines the adiabatic flame temperature, major product species, and laminar burning velocity; the flame stabilizes where the local flow speed matches the burning velocity. In diffusion flames, fuel and oxidizer meet and react by molecular mixing at a thin flame sheet, so local mixing rates control heat release and temperature. These distinctions underpin burner selection, diagnostics, and safety limits such as lean flammability, flashback, and blow-off [10]. In metal-gas hybrid mixtures relevant to this work, experiments in methane-aluminum flames

show a sharp transition from slow particle oxidation to intense, front-like aluminum combustion when the particle loading exceeds approximately ~0.0087-0.0137 $\frac{lb}{ft^3}$ in stoichiometric CH_4-air. Under these conditions, the flame temperature rises toward about 2500 K , and the aluminum combustion front couples to the gas-phase flame [8]. These hybrid effects are central to hardware that disperses aluminum powder into a premixed methane-air stream and require precise control of residence time, heat losses, and diagnostics.

1.2 Different Types of Combustions Test Benches

Quasi-steady powder-burner with Venturi/ejector dispersion. A laboratory dust gas burner that meters powder into a premixed methane air stream using a piston feeder and a high-velocity annular slit or an air-knife to entrain and disperse particles at the throat; optical access at the nozzle enables imaging and laser light attenuation diagnostics. Strengths: continuous/programmable powder feed, close control of particle loading and residence time, and established use in stabilized hybrid flame studies. Limitations: sensitivity to heat losses and flashback; requires careful control of coflow and nozzle boundary conditions [8].

Bunsen heat-flux burners for laminar burning velocity. Bunsen-type cones enable area methods (using total inner-cone surface and volume flow) to infer S_L ; heat-flux burners produce flat, nearly adiabatic, unstretched flames for high-accuracy S_L measurements with embedded thermocouples/heat-flux control. These are ideal for gaseous fuels and extend to hybrid flames with appropriate dispersion systems (piston feeder + flow-knife). Evidence of the piston-feeder/flow-knife approach and the area-method baseline (~1.2 ft/s for stoichiometric methane air) is documented in hybrid methane aluminum studies [8].

Tube-with-quenching-channel assemblies are vertical flame tubes fitted with interchangeable parallel-plate inserts of known gap, allowing direct measurement of the minimum channel width (quenching distance) required for a premixed flame to propagate. In these configurations, the flame is driven upward through the tube and into the channel, and extinction or successful transmission is recorded as a function of gap size, mixture strength, and dust loading. Experiments in hybrid methane–aluminum mixtures show that the quenching distance increases strongly with aluminum concentration; once the particle loading exceeds roughly 0.0087–0.0137 $\frac{lb}{ft^3}$. The aluminum combustion front couples to the gas-phase flame and the merged methane–aluminum flame exhibits a much weaker sensitivity to channel width [7]. This bench-scale configuration is particularly well suited for studying heat losses, flame-wall interaction, and flame-structure changes in hybrid mixtures, but it is not designed to provide controlled steady burning rates or realistic combustor residence times.

Shock tubes and rapid-compression machines are high-temperature, high-pressure transient facilities used to study gas-phase autoignition and reaction kinetics under well-controlled conditions. In a shock tube, a diaphragm rupture generates a propagating shock wave that rapidly raises the temperature and pressure of a test mixture, while in a rapid-compression machine the gas is compressed by a moving piston to similar conditions, creating a nearly homogeneous, adiabatic core. Both devices are routinely instrumented for laser absorption or emission, chemiluminescence, and high-fidelity pressure traces to determine ignition delay times, intermediate-species histories, and overall reaction rates for detailed kinetic mechanism validation [10]. These facilities provide short-duration, spatially uniform T-p-composition states without complications from flow recirculation, heat losses to burner hardware, or multiphase dispersion, yielding fundamental ignition and oxidation data that

complement measurements from steady flames and practical combustors; however, they do not address flameholding, turbulence–flame interaction, or particle dispersion and therefore cannot substitute for burner-scale or system-level design experiments.

Constant-volume dust cloud vessels, typified by the ASTM E1226 20-L sphere, disperse a dust-air cloud uniformly in a sealed, nearly spherical chamber and then ignite it to measure explosion severity. In the standard configuration, a timed dispersion pulse is followed by ignition from a chemical ignitor or spark system, and the resulting pressure-time history is recorded at the vessel wall. From these data, the maximum explosion pressure P_max, maximum rate of pressure rise (dP/dt)_max, dust deflagration index K_st, and minimum explosible concentration (MEC) are determined for a given dust and test protocol, providing a quantitative measure of whether a dust is explosible and how violently it can burn under idealized confinement conditions [12]. The principal strengths of these tests are their standardized geometry, relatively small sample requirements, and highly repeatable data sets for hazard ranking and the design of vents or suppression systems [11,12]. A key limitation is that they generate transient, confined deflagrations whose P_max, K_st, (dP/dt)_max, and MEC values are apparatus-dependent and scale imperfectly to open systems, large process equipment, or complex hybrid gas-dust configurations [11,12].

In this context, a Bunsen-style powder burner offers an attractive platform for hybrid gas-particle combustion studies, providing a stable, attached flame with continuous methane-air flow and well-controlled particle injection. The slender flame and open geometry are well suited for optical diagnostics, while the modular flow path allows systematic variation of dust loading, mixture strength, and nozzle design. These features make a burner configuration a natural choice

for investigating quasi-steady methane-metal dust flames, motivating the dedicated powder-burner test bench developed in this work.

Chapter 2: Design Process

2.1 Design Criteria

The objective of this research is to design a quasi-steady powder burner test bench whose purpose is to study dust cloud combustion. The test bench needs to be able to provide the ability to observe the resulting flame at the burner nozzle and monitor dust concentration. The main goal was not necessarily to verify results from the experiments conducted but rather to deliver a hardware layout and interface necessary to conduct experiments in future studies. The design shall provide the experimenter with precise control over key parameters, including burn rate and the rate of sample introduction into the flow. It shall also ensure repeatability across multiple runs, yielding results within a small margin of error.

2.2 Design Sketch

The system started with a 3D design sketch inside Solidworks with all the ideas and features required for the system. This model was mainly used strictly as a visualization and gave better clarity to plan out the structure of the testbench. This design did not account for any manufacturability and did not include any O-ring that would be supported or needed for the system. Figure 1 below shows a highly detailed description of the parts that consisted in this design with table 1 describing each section and its purpose.

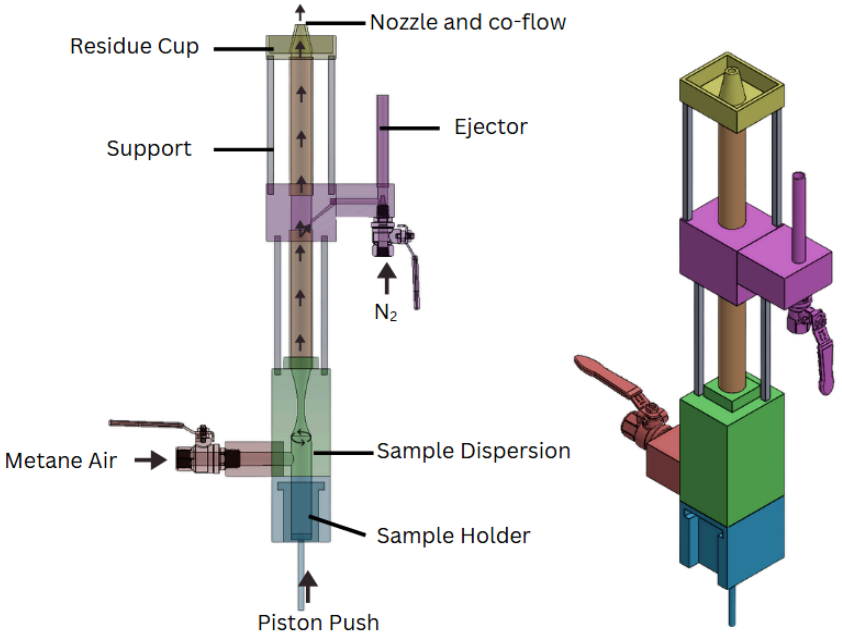

Figure 1. Design schematic of a co-flow burner that uses a piston feed sample to mix with methane air.

Table 1: Summary of the major sections of the experimental system, using color to identify each component in figures and briefly describing its primary function.

Section Name	**Color Correlated**	**Purpose**
Piston System	Blue	Holds samples and introduces them into the methane flow with a piston system.
Flow Body	Green	Merges methane air with the samples to create a mixture and disperse them.
Methane Flow	Red	Introduces methane air.
Flow Control	Pink	Bleeds off a controlled fraction of the mixture using nitrogen gas to keep the operation at constant condition.

Nozzle	Yellow	Shows the flame produced from the mixture.
Flow Tube	Orange	Control the flow upwards.
Support	Grey	Support Structure for the whole system together.

In the blue module, a gear-and-pinion mechanism converts rotary motion into linear actuation, raising the piston to feed samples into the methane flow and control the powder feed rate. Sufficient motor torque is required to overcome friction and lift the piston with its O-ring seal. The O-ring seals the piston-cylinder interface, preventing gas leakage from the co-flow stream, maintaining chamber pressure, and ensuring that the flow rate through the particle burner is well characterized. Torque requirements must therefore be calculated to determine an appropriate motor size.

2.2.1 Motor Torque Requirement

The torque needed from the friction was calculated. The friction force is obtained using the equation below:

$$F_f = \mu \cdot F_n, \quad (1)$$

where F_f is friction force, μ is the coefficient of friction and F_n is the normal force [1]. The normal force was found from the fundamental of definition of pressure $p = \frac{F}{A}$, rearranging the equation gives us the equation below:

$$F_n = p \cdot A \quad (2)$$

where p is the average contact pressure and A is the contact area. In order to determine the contact area is based upon the bore diameter and the O-ring cross section. The equation 3 below factors both into a new equation for F_n:

$$F_n = P_c \cdot (\pi \cdot D \cdot d) \quad (3)$$

where D is the bore diameter and d is the O-ring cross-section diameter. The contact pressure (P_c) in an O-ring seal is determined by the compression exerted between two surfaces: the bore and the piston. Since the O-ring is subjected to compressive loading in this configuration, the contact pressure (P_c) is assumed to be equivalent to the compressive stress (σ) for simplification purposes. This equivalence is an engineering approximation. The actual stresses in the O-ring are nonuniform and may include friction-induced shear. The equation 4 below is for compressive stress taken from Hooke's Law:

$$\sigma = E \cdot \varepsilon, \quad (4)$$

where ε is the normal engineering strain and E is young's modulus of elasticity obtained from data found from data sheets available online [1]. Per the Parker's O-ring handbook [2], the O-ring squeeze is assumed to be equivalent to the strain (ε):

$$Squeeze = \frac{W_o - W_c}{W_o}, \quad (5)$$

with W_o is the original width of the O-ring and W_c is the O-ring gland width to the bore.

After calculating the friction force, the torque can be computed with:

$$T = F_f \times r_p, \quad (6)$$

where T is the torque needed to push the piston and r_p the pitch radius of the gear selected [1].

Table 2 below summarizes all the values and computed values performed using all the equations listed previously.

Table 2: Values and Computed Values

Variable	Terminology	Value	Note
W_o	Original width of the O-ring	0.1464 in	Values taken from selected O-ring [2].
W_c	O-ring gland width to the bore	0.122 in	Values taken from selected O-ring and dimensions from the design sketch 3D model [2].
D	Bore diameter	0.625 in	Dimensions taken from the design sketch 3D model.
d	O-ring cross-section diameter	0.139 in	Values taken from selected O-ring [2].
ε	Squeeze/strain	0.167	
E	Young's modulus	1450 psi	Values taken from ESP International [3].
$\sigma \; or \; P_c$	Compressive stress/ contact pressure	242.15 psi	
F_n	Normal force	66.09 lbf	
μ	Coefficient of friction	0.5 dry and 0.3 lubricant	Values taken from the Pleiger elastomer coefficient of friction [4]. Values are used as conservative estimates.
F_f	Friction force	33.05 lbf	

r_p	Pitch radius of gear	0.375 in	This value is dependent on the gear radius that is selected.
T	Required torque	12.39 lbf-in or 198.24 in-oz	Computed values converted to in-oz for ease of use when finding parts from outside sources.

The required torque calculated is 192.24 in·oz. A factor of safety (FOS) of 2 –3 was adopted, implying a target motor torque of 480.6–576.7 in·oz. The available NEMA-34 stepper provides 467 in·oz holding torque (FOS ≈ 2.43), which is within the recommended range.

2.2.2 Linear Actuator vs Gear and Pinion

During the design of this system, there was a consideration between using gear and pinion or a linear actuator. The table 3 below lists the benefits and disadvantages of each system to push up a piston for the sample section. The reason is because the use of a gear-and-pinion drive in the sample section is considered unreliable: cartridge insertion cannot ensure perfect coaxial alignment, creating lateral side loads that promote rack binding and uneven tooth contact; backlash in the mesh degrades piston positioning accuracy; and the exposed gear train is prone to contamination. A linear actuator is preferred because it provides direct, low-backlash translation with integrated guides that tolerate side loads, precise and repeatable stroke control, sealed construction that resists fouling, and lower maintenance by eliminating exposed gears and external lubricants.

Table 3: Benefits and disadvantages of using a gear and pinion in comparison to a linear actuator.

System	Pros	Cons

Gear and Pinion	- Simple design - Simple sliding mechanic to attach the sample to the motor -Easy maintenance	- Alignment has to be perfect - Reliability - Open system so dust or small particle could jam gear and pinion - Precision limited by gear quality
Linear Actuator	- Good precision and accuracy - Reliable for repetitive testing (consistent) - Smooth motion	- Higher cost - Takes up a lot of space - Less options for loading samples

2.3 First Iteration

The first iteration of the system incorporated a dedicated laser mounting stage that directed the beam through a narrow slit in the nozzle to monitor flow rate. This iteration configuration employs a rack-and-pinion actuator with a specified gear set and motor to characterize the actuation kinematics and torque requirements. Figure 2 provides a detailed view of the assembly.

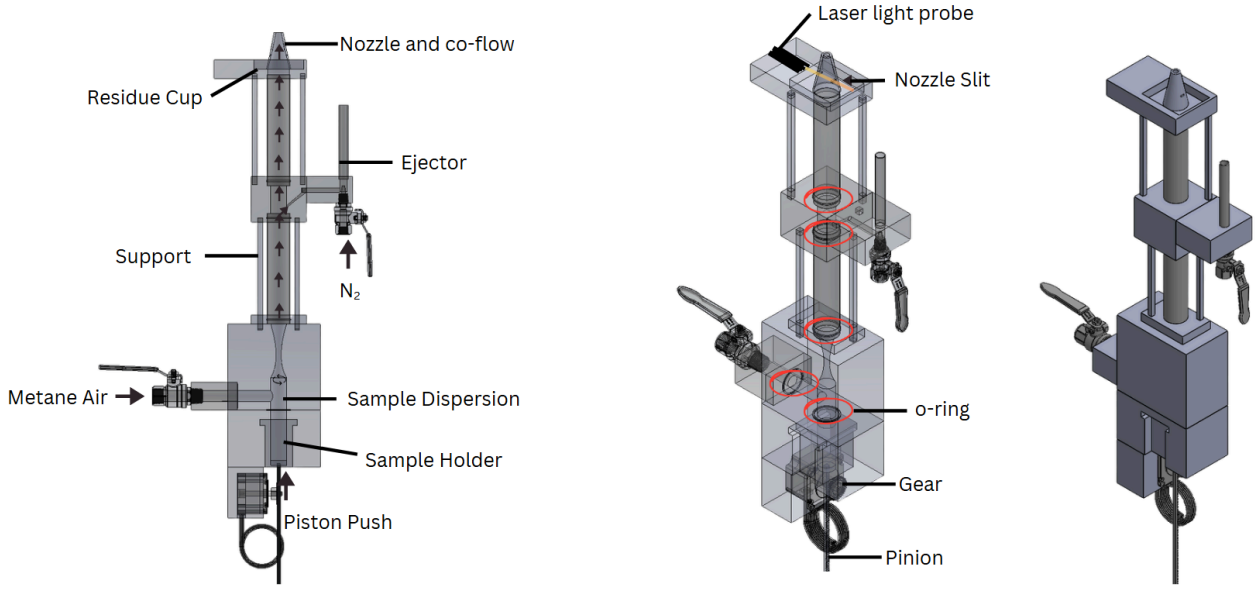

Figure 2. Detailed first iteration design for the entire test bench with fitted O-rings and connections.

This design was an improvement from the design sketch previously adding O-rings to stop any leakage from the flow, specifically an -025 O-ring that is a high-temperature, high-purity silicone O-ring. There was not a significant amount of changes that was made in this iteration from the design sketch but a notable highlight is the removable sample container shown in figure 3.

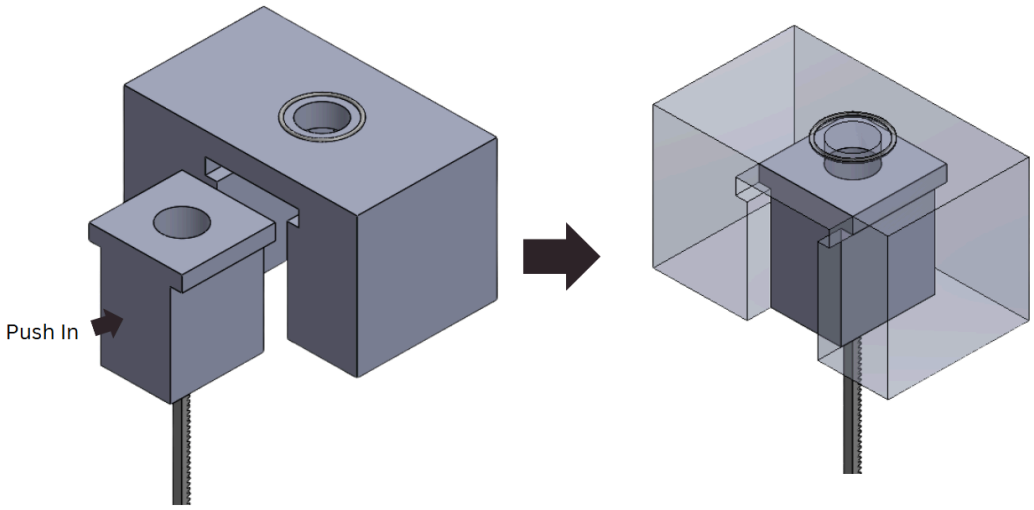

Figure 3. Demonstration of a sliding sample container into its housing to be pushed up and introduced in the flow.

Throughout other different iterations, making a feature where samples could be loaded in easily is one of the main goals. For the case of this iteration it was a sliding feature to load the samples in. This feature though is very simple it lacks the ability to make a seal connection between the sample container and the body leading to leakage and manufacturability. A different approach had to be used.

2.4 Second Iteration

The second iteration's focus was manufacturability and reduction of wasted material. No motor is shown in figure 4. The gears and pinion introduced multiple integration challenges when integrated into the first iteration system design. The reason was reliability and alignment sensitivity. The pinion must be kept very close to perfectly aligned with the gear, with tight control of center distance, uneven tooth contact can cause the whole system to fail. In addition, when the gear rotates it imparts a line-of-action force that tends to translate the pinion along its guide, so a constant axial preload is required to keep the teeth fully engaged and to prevent the pinion from being driven forward/out of mesh. This leads to non-uniform upward motion, which is critical when running multiple trials where consistency is the priority.

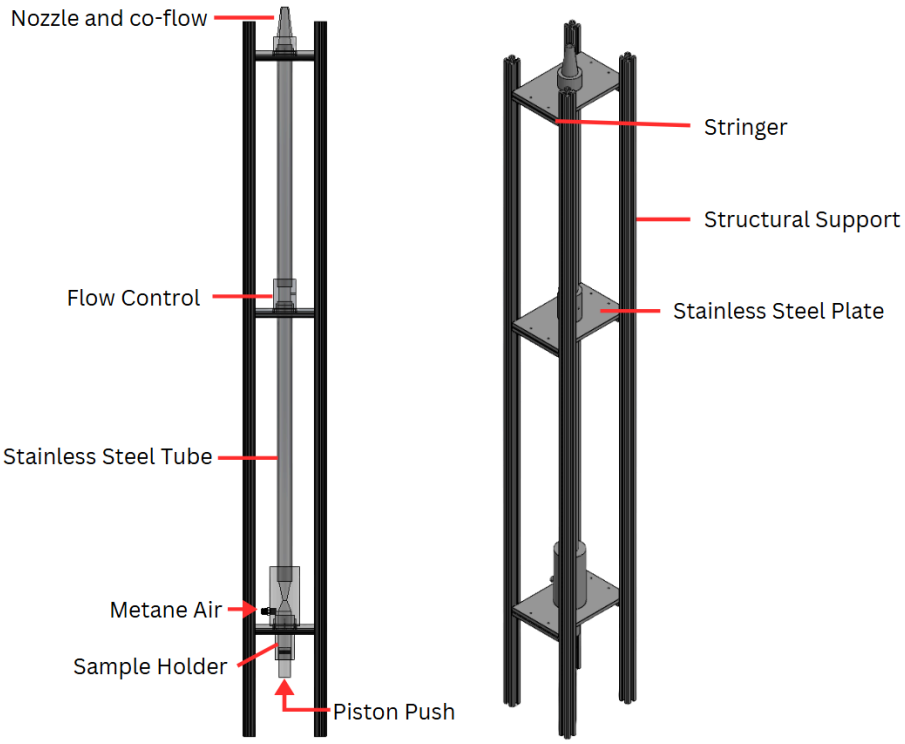

Figure 4. Second iteration of the test bench design focusing on manufacturability with detailed parts and description.

The bottom section consists of the methane air flow, the sample container, piston, and flowbody. The main focus of this section is to mix the samples into the methane air flow stream. An air knife is used to create a circular motion up the flow nozzle dispersing the flow upstream, referring to figure 5 this is done by using an orifice that has a 0.01 inch diameter hole.

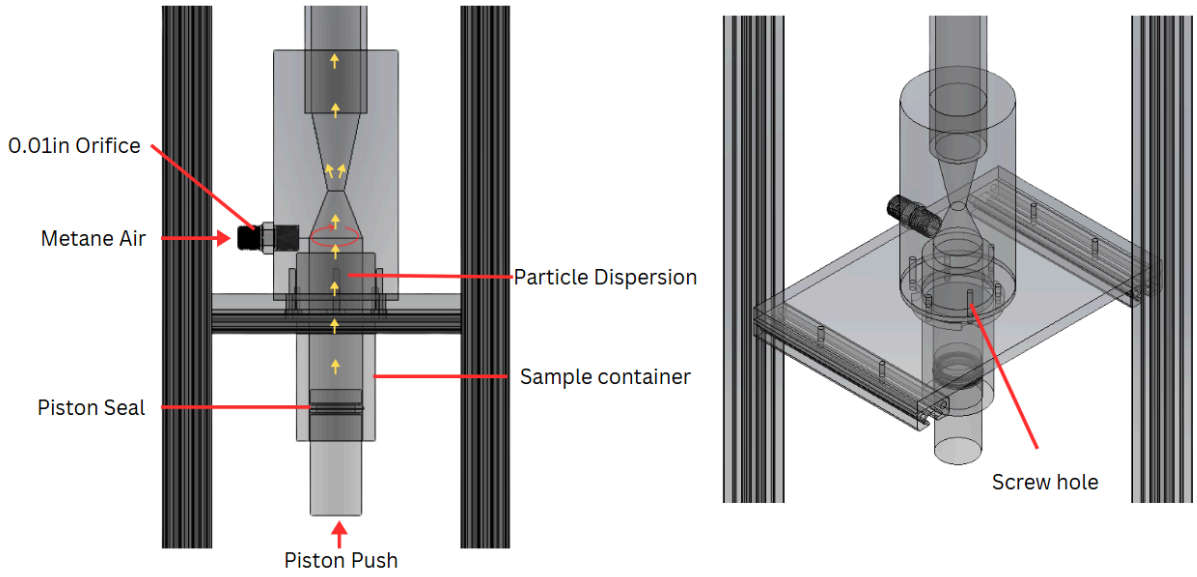

Figure 5. Bottom flow section showing the particle dispersion chamber and sample piston elevator.

The remaining major components are the middle flow controller and the top burner nozzle, shown in Figure 6. The middle flow controller is intended to bleed off or redirect a portion of the upward mixture, while the nozzle shapes and discharges the emerging flame. However, due to time constraints, the present work focused primarily on the bottom flow section; as a result, the middle and top sections were implemented as simplified placeholder geometries to guide future, more detailed design and testing.

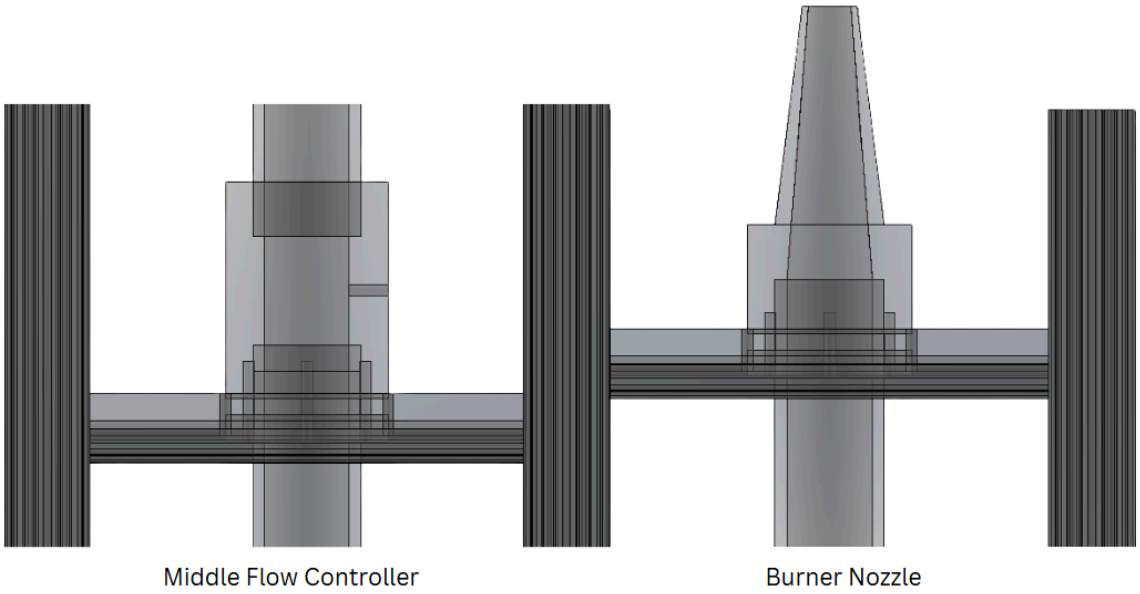

Figure 6. Middle flow control section to control the flow mixture and the burner nozzle.

2.5 Third Iteration

The third iteration mainly focused on the bottom sample section of the system. The main idea of this choice was to develop the design further and get an almost fully operational design. A linear actuator was decided to be used instead of the gears and pinion system since it has a consistent vertical motion up and down. Figure 7 shows that idea. A stainless steel pipe was replacing the previous stainless steel tube from the previous design. The reason why the pipe was chosen was because it could be connected with a flange and enclosed with bolts to an O-ring to seal as opposed to the previous welding which would make connections permanent. This design also features a 0.01 inch diameter orifice which was the smallest hole that was found to be commercially available.

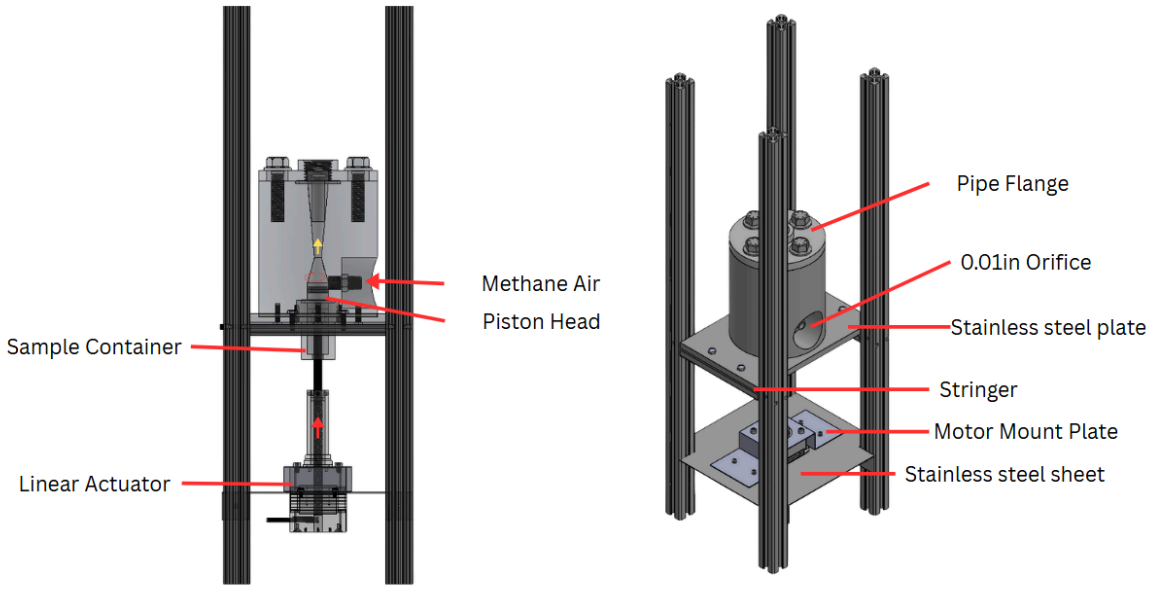

Figure 7. Third iteration schematic focusing on the flowbody and the piston loading section.

One of the main concerns for this design was that the gap between the sample container and the main body was too small as demonstrated in figure 8. The gap might cause difficulties when loading in samples which lead to a major change of design in iteration four.

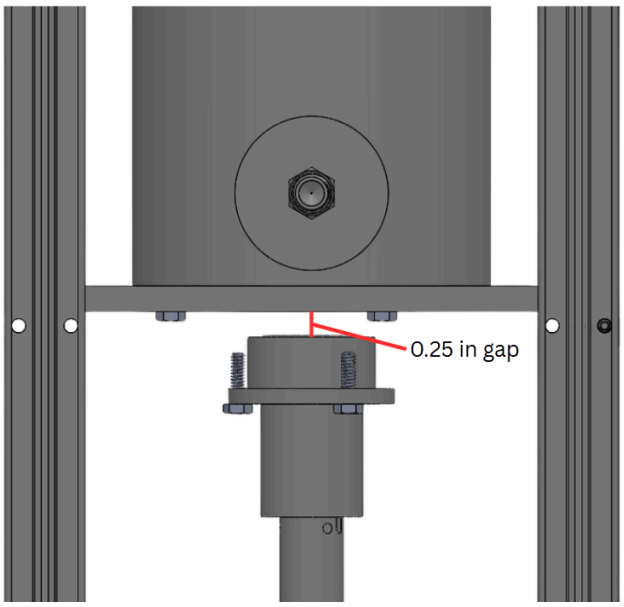

Figure 8. Sample container with a small gap between the cup and flowbody.

2.6 Fourth Iteration

In the fourth iteration (Figure 9), the external frame was reconfigured into a three-post structure to open the front of the rig and improve access to the sample section. A vertical sliding carriage was added for the motor and piston assembly so the drive unit can be raised during loading to create sufficient clearance between the piston, sample holder, and flow body. After the samples are inserted, the carriage is lowered back to its indexed operating position, ensuring proper alignment while still providing the additional space needed for safe, repeatable sample loading.

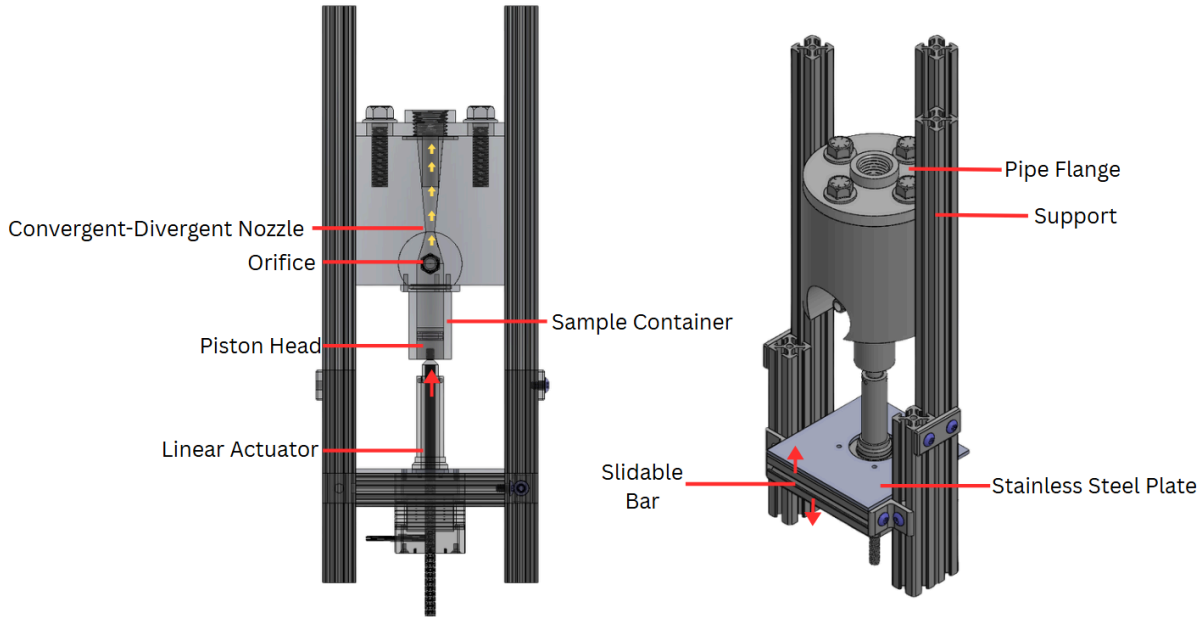

Figure 9. Fourth iteration schematic addressing the spacing issue of the previous iteration.

This fourth iteration was the design that was selected and it will be explained in greater details in chapter 3.

Chapter 3: Final Design Selection

3.1 Selection

After multiple design iterations, the fourth and final configuration was selected. The primary requirement was precise control over the burn rate and sample introduction. This was achieved with a variable speed linear actuator. The choice of a linear actuator provides a reliable and repeatable motion across successive runs, which ensures consistent results.

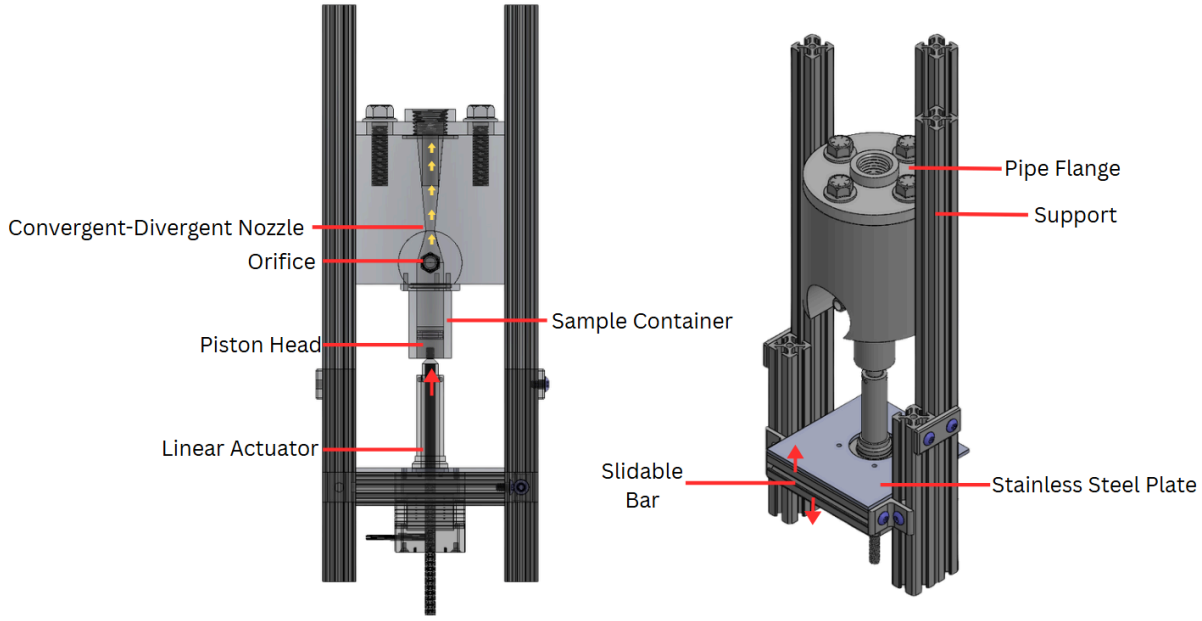

Figure 9. Fourth iteration schematic addressing the spacing issue of the previous iteration.

3.2 Features

One of the main features of this system was a sliding bottom section. These features allow for the hex screws to be loosened and pull the section down to leave a big enough space to load in any samples. This feature allows for a gap that is 1.25 inches which provides sufficient enough space to load the sample in with ease. Figure 10 below demonstrates this feature.

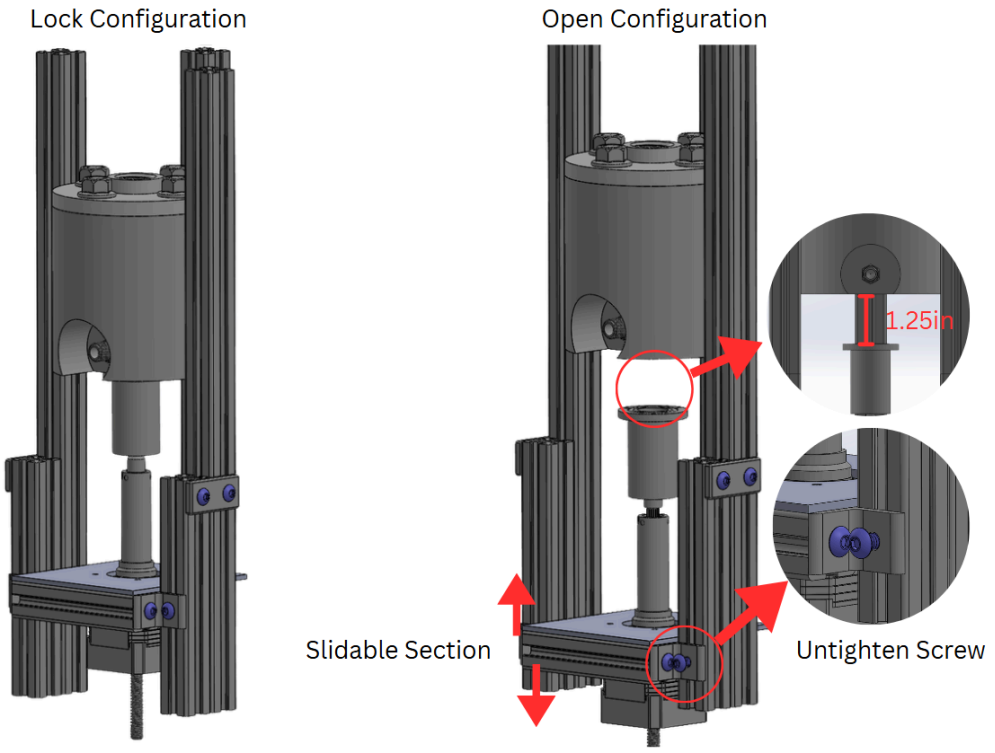

Figure 10. Sliding feature demonstration of the sample platform.

The next feature of the system is a converging-diverging Venturi nozzle configured as an ejector mixer. The methane air stream is delivered through an orifice, forming an air knife that sweeps the throat with a thin high velocity layer of methane. A piston advances the sample upward and introduces it through the bottom inlet. The low pressure at the throat draws the sample into the core jet, where it is entrained and mixed with the methane, then carried into the diverging section for expansion. The air knife keeps the entry clear and promotes fast, uniform mixing [5]. Figure 11 below conveys this feature.

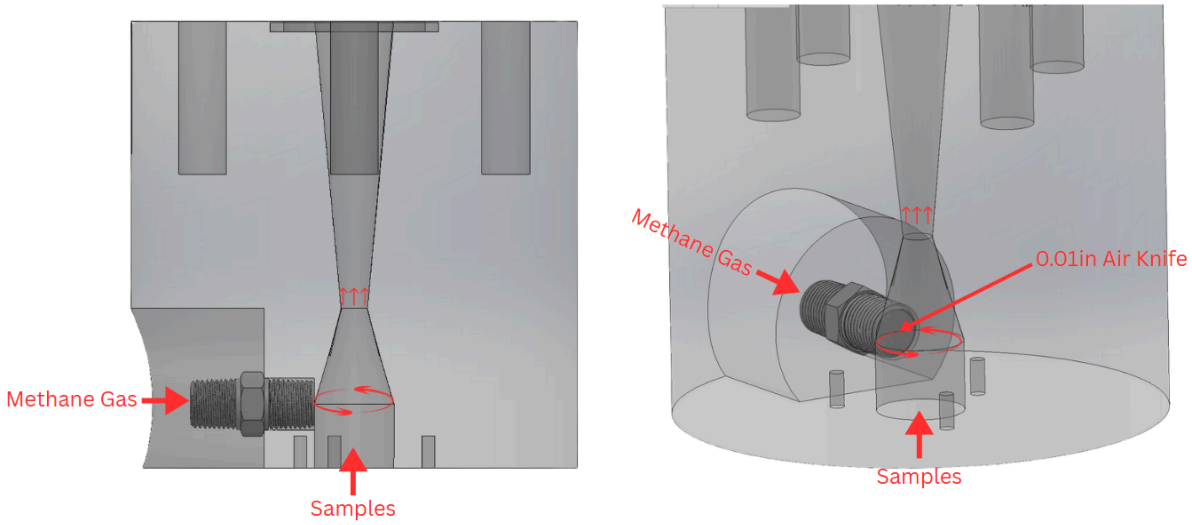

Figure 11. Flow demonstration of samples coming in from the container mixing with methane gas.

3.3 System's Frame

The structural assembly consists of three primary extruded aluminum frames welded to the flow body, creating a rigid and permanent backbone for the test bench. Two shorter frames of equal length are then attached to the primaries with a bolted structural bracket using button head screws, providing a secure but removable connection. This layout separates functions: the welded members establish alignment and carry the principal loads, while the bracketed subassembly can be detached for maintenance, transport, or component replacement without disturbing the welded joints. Figure 12 identifies the primary frames, short frames, and the bracket hardware.

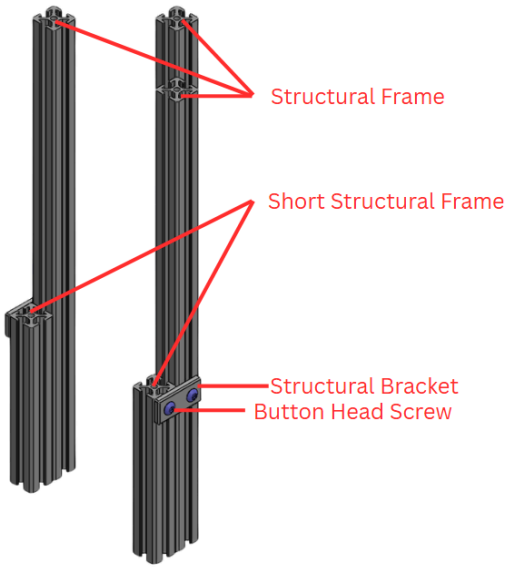

Figure 12. Structural beam to support the whole system setup.

3.4 Flow Body

The flow body houses a central passage that guides the piston driven sample into the main gas stream. A standard pipe flange at the inlet provides a rigid, leak tight interface to the supply manifold and allows quick removal for inspection and cleaning. Injection occurs through a precision 0.01 inch hole acting as a flow knife, which introduces the sample cleanly and centrally into the flow so it travels up the pipe into the middle section and, ultimately, the burner. To achieve such a small injection opening, the design uses a commercial micro-orifice rather than drilling the passage directly. CNC tooling could not reliably produce the originally targeted 0.0016 inch feature, so the smallest practical option was a 0.01 inch orifice, which was selected and installed as the flow knife element. This choice provides a well defined geometry and predictable metering characteristics for repeatable tests, and it also makes maintenance simpler

since the orifice can be replaced or resized as needed. Figure 13 below shows a view of all the components connected to the flow body.

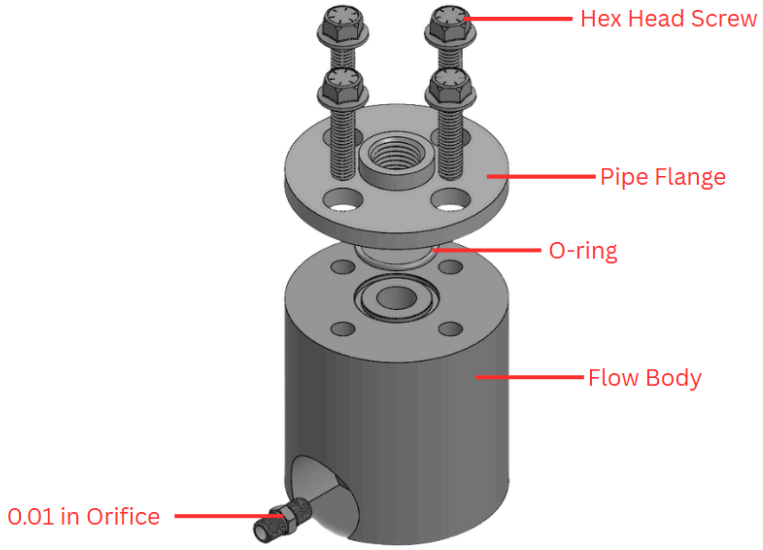

Figure 13. Components breakdown for the flow body section.

3.5 Sample Elevator

The sample elevator consists of the sample container, piston head, linear actuator, and a moving platform that mounts the linear actuator to the platform. The sample elevator is a section that is movable up and down by tightening and untightening the button head screw. As a safety feature it also has a screwed connection between the sample container and flow body to ensure a sealed connection. The figure below will demonstrate a general layout and the subsections will breakdown the system further.

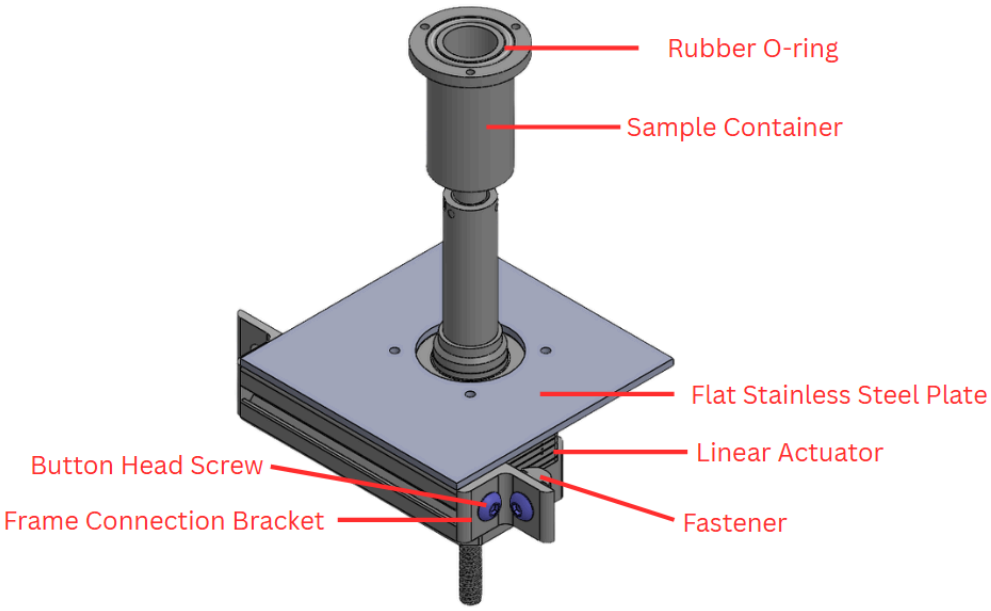

Figure 14. Components break down for the sample elevator section.

3.5.1 Sample Container & Linear Actuator

The sample container is connected to the flow body with screws that can be tightened after sliding the bottom section upwards. The linear actuator has a screwable tip that is then screwed to the piston head and it can safely push up samples without any spillage because of the piston O-ring stopping it. The figure below shows a descriptive view of the components

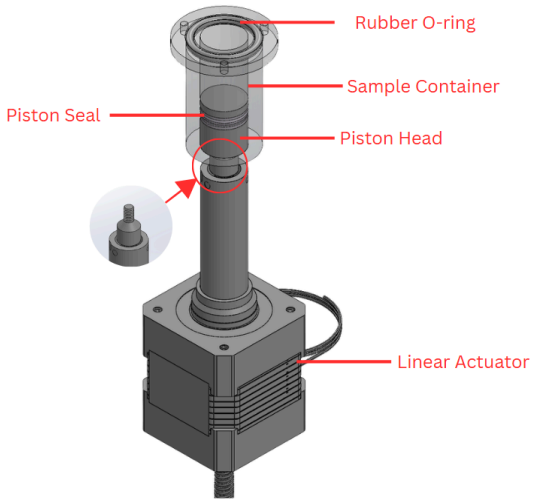

Figure 15. Components breakdown for the sample and linear actuator.

3.5.2 Sliding Platform

The sliding platform features a small structural bar that is welded to the stainless steel plate to create a permanent part ensuring a sturdy platform. The bar is then screwed to the frame connection bracket with a hex head screw to secure it and another hex screw will be fastened to the small structural frame mentioned in the system's frame section with a fastener inside.

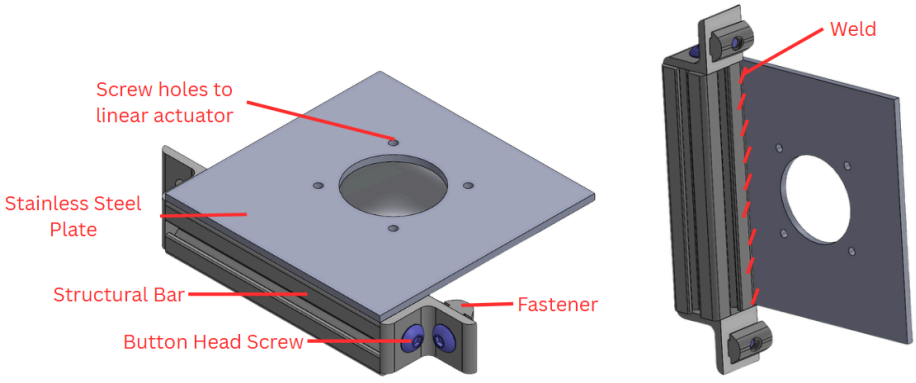

Figure 16. Descriptive figure of the sliding platform and the connections between the bar and the plate.

Chapter 4: Recommendations

4.1 Current State and Future Work

Over the past one and a half semesters the work focused’./ on developing a thorough design for the test bench with the intent to reach an operational baseline and proceed to machining and assembly. That milestone was not reached within the available time, so fabrication and build activities are deferred to a later future. The current design delivers a complete bottom section that incorporates the critical features of the system, including the structural frame, flow body, sample sliding section, and sealing interfaces. Models, clearances, and assembly order have been defined in CAD and drawings, with key interface tolerances documented in the appendix below, and the approach has been checked for manufacturability and service access. Two elements still require a full design: the top flow control section and burner nozzle. Interface geometry and connection strategy between these modules and the completed base are shown in the design sketch and in several iterations, providing a clear path to integration and idea. Future next steps should include finishing those two sections mentioned and preparing procedures for machining, assembly, and verification.

4.2 Summary

This work established the engineering basis for a quasi steady powder burner test bench and delivered a complete, manufacturable design for the bottom section. The final configuration integrates a rigid three post frame, a serviceable flow body with a flanged joint, and a sample elevator driven by a linear actuator mounted on a sliding platform for easy loading. The mixing approach relies on a converging-diverging Venturi nozzle with a commercial 0.01 inch micro

orifice that forms an air knife to entrain and disperse the sample, providing clear geometry and predictable metering. The design progression, torque sizing for the actuator, and key interfaces are documented and illustrated in the figures.

Appendix

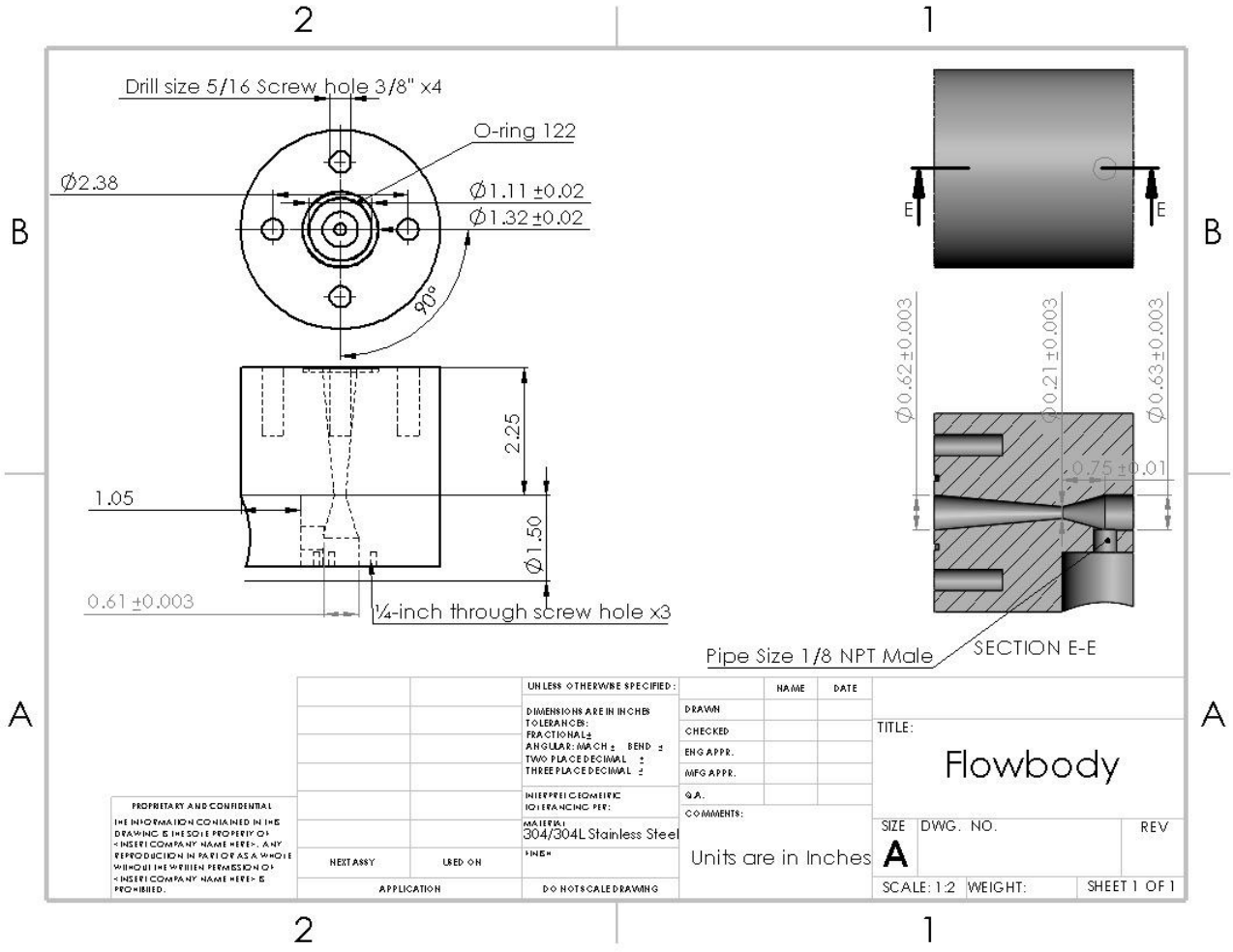
Drill size 5/16 Screw hole 3/8" x4
O-ring 122
Ø2.38
Ø1.11 ±0.02
Ø1.32 ±0.02
90°
2.25
1.05
Ø1.50
0.61 ±0.003
¼-inch through screw hole x3
E
E
Ø0.62±0.003
Ø0.21±0.003
Ø0.63±0.003
0.75±0.01
Pipe Size 1/8 NPT Male
SECTION E-E
UNLESS OTHERWISE SPECIFIED:
DIMENSIONS ARE IN INCHES
TOLERANCES:
FRACTIONAL ±
ANGULAR: MACH ± BEND ±
TWO PLACE DECIMAL ±
THREE PLACE DECIMAL ±
INTERPRET GEOMETRIC TOLERANCING PER:
MATERIAL
304/304L Stainless Steel
FINISH
DO NOT SCALE DRAWING
NAME
DATE
DRAWN
CHECKED
ENG APPR.
MFG APPR.
Q.A.
COMMENTS:
Units are in Inches
TITLE:
Flowbody
SIZE
A
DWG. NO.
REV
SCALE: 1:2
WEIGHT:
SHEET 1 OF 1
NEXT ASSY
USED ON
APPLICATION
PROPRIETARY AND CONFIDENTIAL
THE INFORMATION CONTAINED IN THIS DRAWING IS THE SOLE PROPERTY OF <INSERT COMPANY NAME HERE>. ANY REPRODUCTION IN PART OR AS A WHOLE WITHOUT THE WRITTEN PERMISSION OF <INSERT COMPANY NAME HERE> IS PROHIBITED.

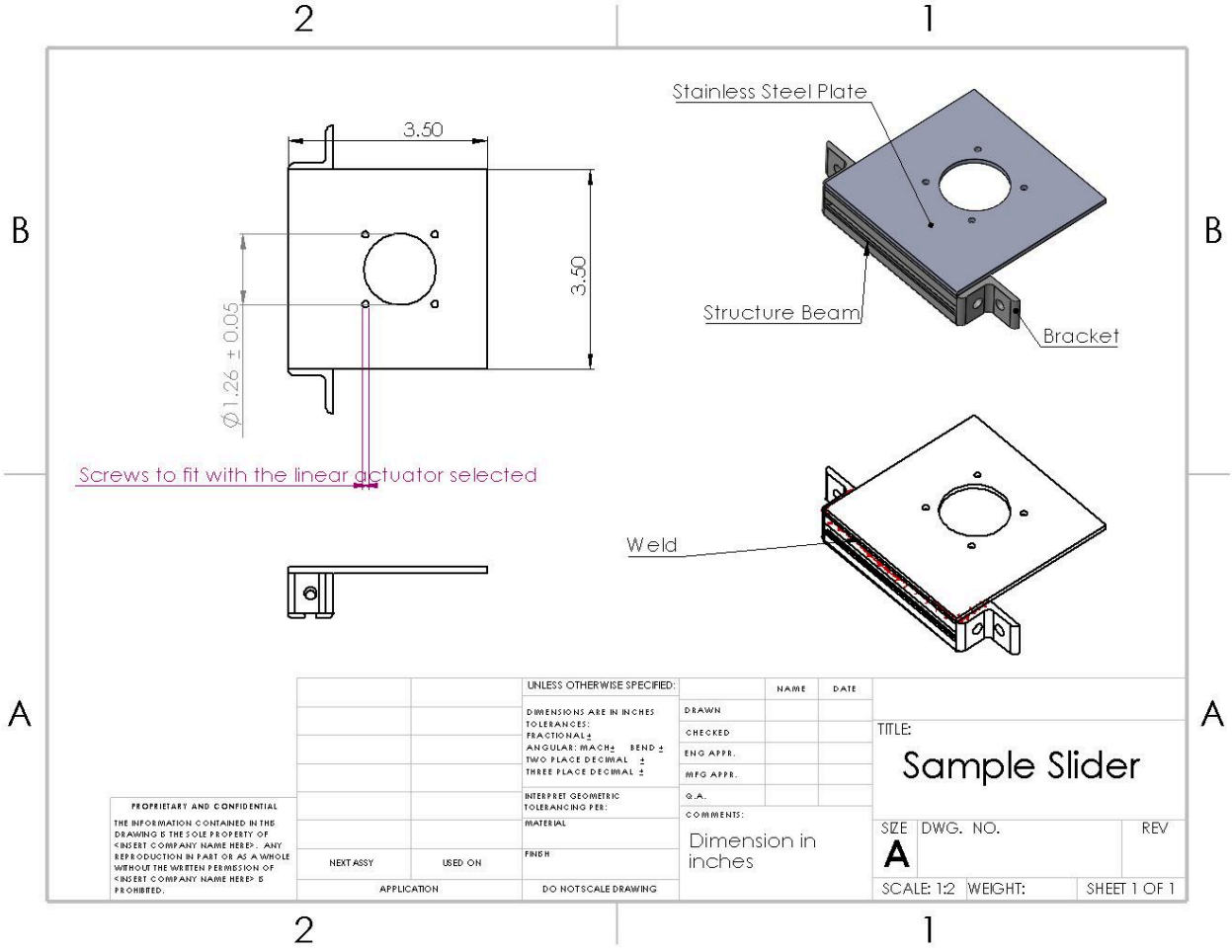
2
1
B
A
3.50
3.50
Ø1.26 ± 0.05
Screws to fit with the linear actuator selected
Stainless Steel Plate
Structure Beam
Bracket
Weld
UNLESS OTHERWISE SPECIFIED:
DIMENSIONS ARE IN INCHES
TOLERANCES:
FRACTIONAL ±
ANGULAR: MACH ± BEND ±
TWO PLACE DECIMAL ±
THREE PLACE DECIMAL ±
INTERPRET GEOMETRIC TOLERANCING PER:
MATERIAL
FINISH
NEXT ASSY
USED ON
APPLICATION
DO NOT SCALE DRAWING
NAME
DATE
DRAWN
CHECKED
ENG APPR.
MFG APPR.
Q.A.
COMMENTS:
Dimension in inches
TITLE:
Sample Slider
SIZE
A
DWG. NO.
REV
SCALE: 1:2
WEIGHT:
SHEET 1 OF 1
PROPRIETARY AND CONFIDENTIAL
THE INFORMATION CONTAINED IN THIS DRAWING IS THE SOLE PROPERTY OF <INSERT COMPANY NAME HERE>. ANY REPRODUCTION IN PART OR AS A WHOLE WITHOUT THE WRITTEN PERMISSION OF <INSERT COMPANY NAME HERE> IS PROHIBITED.

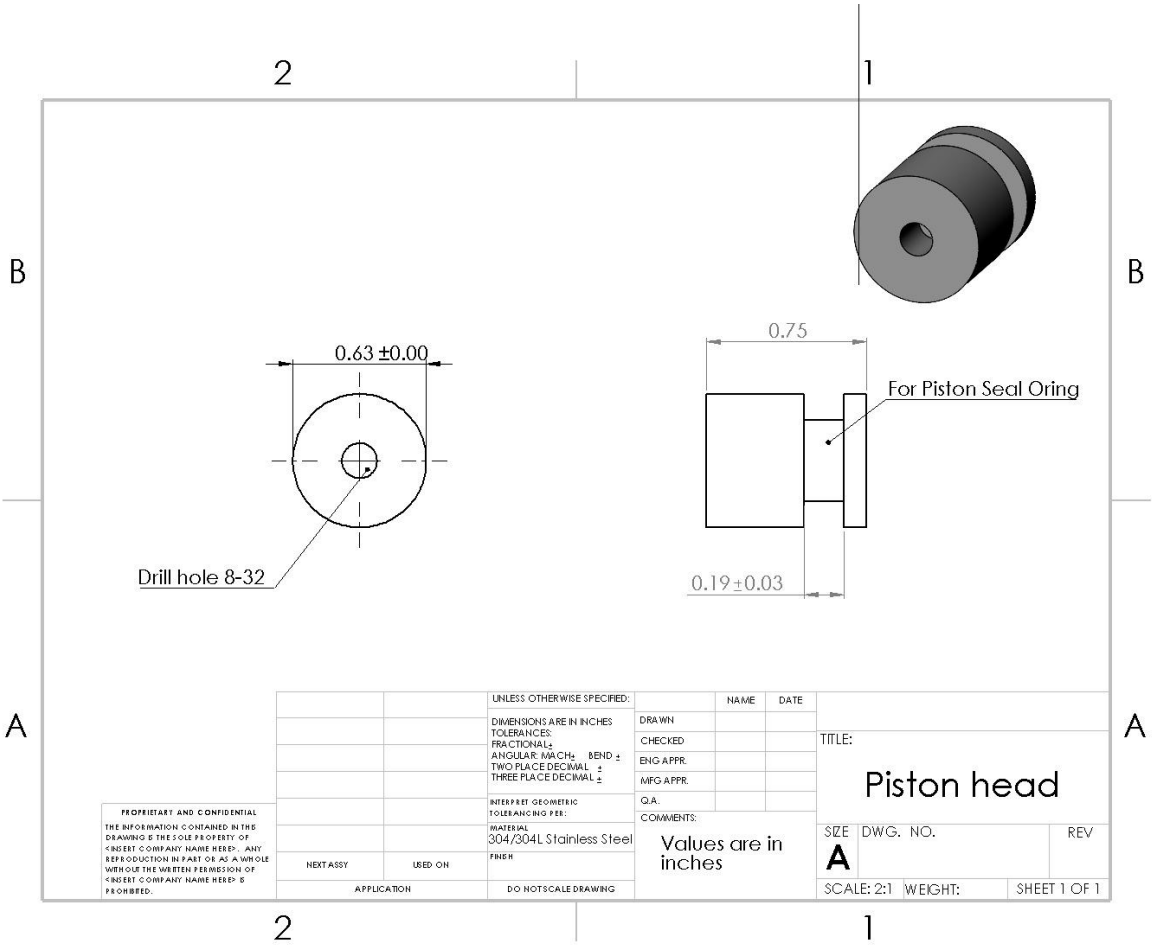
2
1
B
B
A
A
0.63 ±0.00
Drill hole 8-32
0.75
For Piston Seal Oring
0.19±0.03
UNLESS OTHERWISE SPECIFIED:
DIMENSIONS ARE IN INCHES
TOLERANCES:
FRACTIONAL ±
ANGULAR: MACH ± BEND ±
TWO PLACE DECIMAL ±
THREE PLACE DECIMAL ±
INTERPRET GEOMETRIC TOLERANCING PER:
MATERIAL
304/304L Stainless Steel
FINISH
NEXT ASSY
USED ON
APPLICATION
DO NOT SCALE DRAWING
NAME
DATE
DRAWN
CHECKED
ENG APPR.
MFG APPR.
Q.A.
COMMENTS:
Values are in inches
TITLE:
Piston head
SIZE
A
DWG. NO.
REV
SCALE: 2:1
WEIGHT:
SHEET 1 OF 1
PROPRIETARY AND CONFIDENTIAL
THE INFORMATION CONTAINED IN THIS DRAWING IS THE SOLE PROPERTY OF <INSERT COMPANY NAME HERE>. ANY REPRODUCTION IN PART OR AS A WHOLE WITHOUT THE WRITTEN PERMISSION OF <INSERT COMPANY NAME HERE> IS PROHIBITED.

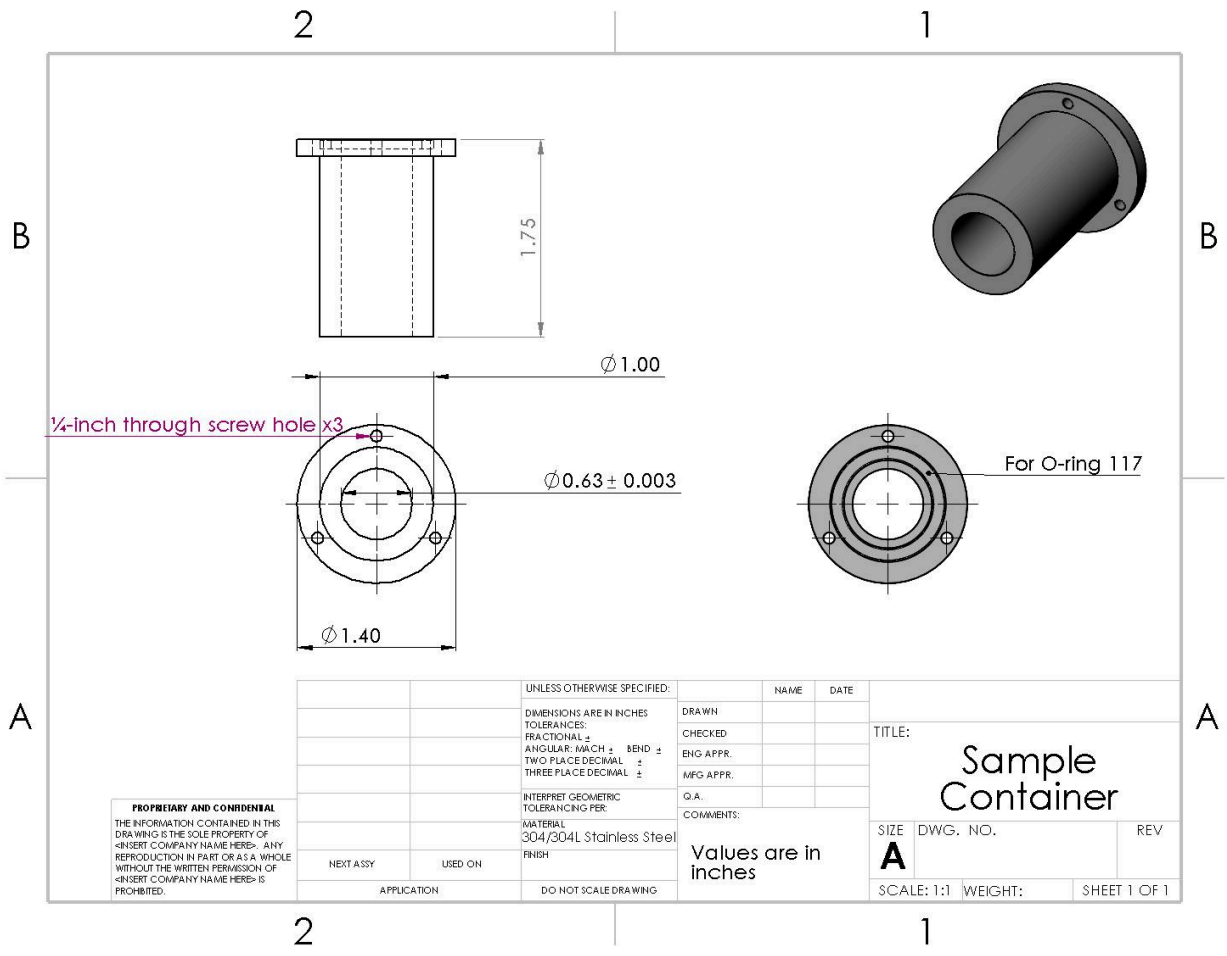
2
1
B
B
1.75
∅1.00
¼-inch through screw hole x3
∅0.63 ± 0.003
For O-ring 117
∅1.40
A
A
UNLESS OTHERWISE SPECIFIED:
DIMENSIONS ARE IN INCHES
TOLERANCES:
FRACTIONAL ±
ANGULAR: MACH ± BEND ±
TWO PLACE DECIMAL ±
THREE PLACE DECIMAL ±
INTERPRET GEOMETRIC TOLERANCING PER:
MATERIAL
304/304L Stainless Steel
FINISH
DO NOT SCALE DRAWING
NAME
DATE
DRAWN
CHECKED
ENG APPR.
MFG APPR.
Q.A.
COMMENTS:
Values are in inches
TITLE:
Sample Container
SIZE
A
DWG. NO.
REV
SCALE: 1:1
WEIGHT:
SHEET 1 OF 1
PROPRIETARY AND CONFIDENTIAL
THE INFORMATION CONTAINED IN THIS DRAWING IS THE SOLE PROPERTY OF <INSERT COMPANY NAME HERE>. ANY REPRODUCTION IN PART OR AS A WHOLE WITHOUT THE WRITTEN PERMISSION OF <INSERT COMPANY NAME HERE> IS PROHIBITED.
NEXT ASSY
USED ON
APPLICATION
2
1

References

[1] Budynas, R. G., & Nisbett, J. K. (2015). *Shigley's Mechanical Engineering Design* (10th ed.). McGraw-Hill Education.

[2] Parker Hannifin Corporation. (2021). Parker O-Ring Handbook. https://www.parker.com/us/en/home.html

[3] ESP International. (n.d.). *Parker NBR N1470-70 O-Rings*. https://www.espint.com/o-rings/nitrile-nbr/parker-nbr-n1470-o-rings

[4] Pleiger Plastics Company. (2017). *Elastomer Coefficient of Friction*. https://pleiger.com/wp-content/uploads/2022/04/Coefficient-of-Friction.pdf

[5] Anderson, J. D. (2017). *Fundamentals of Aerodynamics* (6th ed.). McGraw-Hill Education.

[6] Fedoryk, M., Stelzner, B., Harth, S., & Trimis, D. (2023). *Experimental investigation of the laminar burning velocity of iron–air flames in a tube burner*. *Applications in Energy and Combustion Science, 13*(100111). Elsevier. https://doi.org/10.1016/j.jaecs.2022.100111

[7] Palecka, J., Julien, P., Goroshin, S., Bergthorson, J. M., Frost, D. L., & Higgins, A. J. (2015). *Quenching distance of flames in hybrid methane–aluminum mixtures*. *Proceedings of the Combustion Institute, 35*(3), 2463–2470. https://doi.org/10.1016/j.proci.2014.06.116

[8] Soo, M., Julien, P., Goroshin, S., Bergthorson, J. M., & Frost, D. L. (2013). *Stabilized flames in hybrid aluminum–methane–air mixtures*. *Proceedings of the Combustion Institute, 34*(2), 2213–2220. https://doi.org/10.1016/j.proci.2012.05.044

[9] Glassman, I., Yetter, R. A., & Glumac, N. G. (2015). *Combustion* (5th ed.). Academic Press.

[10] Turns, S. R. (2021). *An Introduction to Combustion: Concepts and Applications* (4th ed.). McGraw-Hill Education.

[11] Kalman, J. (2014). *Experimental investigation of constant volume sulfur dust explosions* (Doctoral dissertation, University of Illinois Urbana-Champaign). IDEALS. https://hdl.handle.net/2142/50508.

[12] ASTM International. (2019). *ASTM E1226-19: Standard test method for explosibility of dust clouds*. West Conshohocken, PA: ASTM International. https://www.astm.org/e1226-19.html.